nature cell biology

Tensile forces govern germ-layer organization in zebrafish

M. Krieg[1], Y. Arboleda-Estudillo[1,2], P.-H. Puech[3], J. Käfer[4], F. Graner[4], D. J. Müller[1,5] and C.-P. Heisenberg[2,5]

Understanding the factors that direct tissue organization during development is one of the most fundamental goals in developmental biology. Various hypotheses explain cell sorting and tissue organization on the basis of the adhesive and mechanical properties of the constituent cells[1]. However, validating these hypotheses has been difficult due to the lack of appropriate tools to measure these parameters. Here we use atomic force microscopy (AFM) to quantify the adhesive and mechanical properties of individual ectoderm, mesoderm and endoderm progenitor cells from gastrulating zebrafish embryos. Combining these data with tissue self-assembly *in vitro* and the sorting behaviour of progenitors *in vivo*, we have shown that differential actomyosin-dependent cell-cortex tension, regulated by Nodal/TGFβ-signalling (transforming growth factor β), constitutes a key factor that directs progenitor-cell sorting. These results demonstrate a previously unrecognized role for Nodal-controlled cell-cortex tension in germ-layer organization during gastrulation.

Gastrulation is the first stage in vertebrate development when different progenitor types sort-out and assemble into distinct germ layers[2]. Both cell adhesion and contraction have long been implicated in germ-layer formation; however, their relative contribution to these processes is still a matter of debate[3]. We therefore sought to quantify the specific adhesive and mechanical properties of the different progenitor types at the single-cell level and correlate these values to the actual sorting behaviour of progenitors *in vitro* and *in vivo* (for generation of different germ-layer progenitor types see Supplementary Information, Fig. S1 and Methods).

To measure cell adhesion at the single-cell level, we used an atomic force microscope (AFM) as a single-cell force spectroscope (SCFS; Fig. 1a; refs 4–6). Adhesion forces between two isolated zebrafish germ-layer cells were measured by bringing the cells into contact until a pre-defined force was reached and then recording the force needed to separate them after a given dwell-time, which ranged from 1–60 s. When adhesion forces between progenitors of the same type (homotypic adhesion; 'cohesion') were measured, ectoderm progenitors showed significantly less cohesion compared with their mesoderm and endoderm counterparts for all contact times tested (Fig.1b; Supplementary Information, Table S1, Fig. S2a, b). Adhesive forces between different progenitor types (heterotypic adhesion) were similar to homotypic cell contacts of ectoderm cells, the least cohesive cell type (Fig. 1c). The recorded differences in cell–cell adhesion are unlikely to be a consequence of dissimilar morphological and/or mechanical cell-properties, as neither cell size (Supplementary Information, Fig. S2c) nor 'contact stiffness' correlated with the recorded maximum adhesion forces ($r = 0.14$, Fig. 1d; see also Methods). Taken together, these observations demonstrate that mesoderm and endoderm progenitors are more cohesive than ectoderm cells.

Cadherin adhesion molecules, particularly E-cadherin, are known to have key roles in tissue morphogenesis during vertebrate gastrulation[7]. To test whether E-cadherin is involved in differential cohesion of germ-layer progenitors, we measured cohesion when E-cadherin function was impaired. Cohesion of all three progenitor types was markedly reduced when calcium ions were depleted from the medium and, more specifically, when E-cadherin expression was knocked down using morpholino antisense oligonucleotides (Fig. 1e), indicating that E-cadherin mediates progenitor-cell cohesion. To test whether the progenitors show differences in cadherin-mediated adhesion that are similar to their differential cohesive properties, we measured the adhesion of ectoderm, mesoderm and endoderm progenitors to substrates coated with E-cadherin[8]. Mesoderm and endoderm progenitors adhered more to E-cadherin substrates than ectoderm cells (Supplementary Information, Fig. S2d), indicating that adhesion of progenitors to cadherins correlates with their cohesive properties. Consistently, we found that in embryos at the onset of gastrulation (6 h post fertilization; hpf), E-cadherin density at the plasma membrane of mesendoderm (mesoderm and endoderm) progenitors was higher than in the directly adjacent ectoderm progenitors (Fig. 1f; Supplementary Information, Fig. S2e; ref. 9). Similarly, the amount of classical cadherins at the plasma membrane of dissociated ectoderm progenitors, detected by an anti-pan-cadherin antibody[10] on western blots, was lower than in mesoderm and endoderm cells (Fig. 1f′). Together, these findings demonstrate that differential cohesion of germ-layer progenitors is mediated primarily by classical cadherins including E-cadherin.

In addition to differential adhesion, differential cell contraction has been implicated in cell sorting and tissue self-assembly[11]. Studies using

[1]BIOTEC, Technische Universität Dresden, Tatzberg 47-51, 01307 Dresden, Germany. [2]Max-Planck-Institute for Molecular Cell Biology and Genetics, Pfotenhauerstr.108, 01307 Dresden, Germany. [3]INSERM/UMR 600, CNRS/UMR6212, Case 937, 163 Avenue de Luminy, 13288 Marseille, France. [4]Laboratoire de Spectrométrie Physique, UMR 5588, UJF Grenoble I & CNRS, 140 Avenue de la Physique, 38402 Saint Martin d'Hères, France.
[5]Correspondence should be addressd to C.-P.H or D.J.M. (e-mail: heisenberg@mpi-cbg.de; mueller@biotec.tu-dresden.de)

Received 19 October 2007; accepted 28 January 2008; published online 23 March 2008; DOI: 10.1038/ncb1705

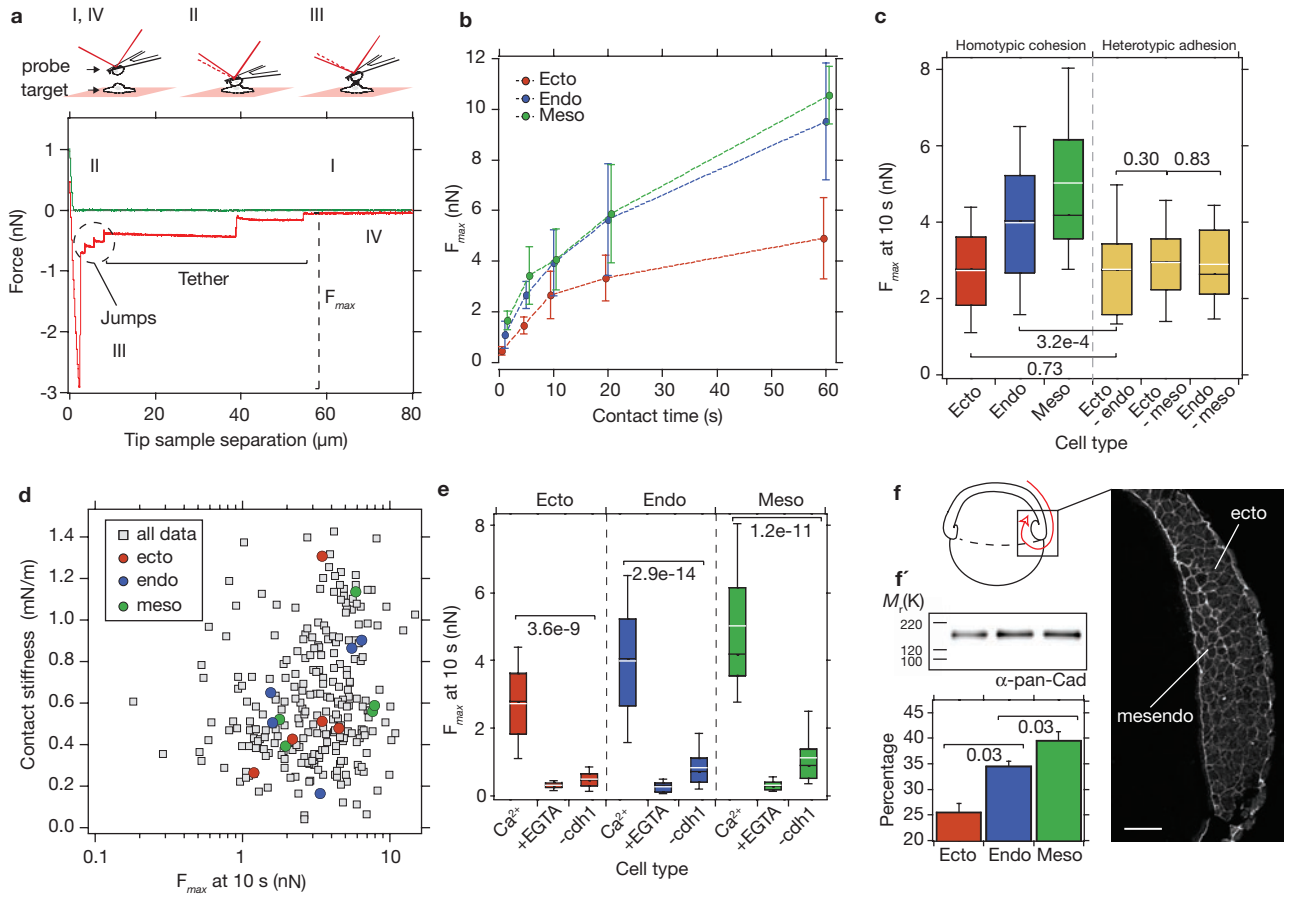

Figure 1 Adhesion of germ-layer progenitors measured by single-cell force spectroscopy (SCFS). (**a**) Outline of the SCFS adhesion assay. One cell immobilized on an AFM cantilever (probe) is brought into contact at a given speed with a second cell adhering to a solid substrate (target). After a predefined contact time, the cell was retracted at the same speed and the interaction force was detected by the cantilever deflection. The resultant force-distance curve allows quantification of the maximum adhesion force (F_{max}). (**b**) F_{max} as a function of contact time for homotypic adhesion between the three different progenitor types. Values are presented as median ± MAD. For detailed representations of the statistics see Supplementary Information, Fig. S2a, b, Table S1. (**c**) Homotypic versus heterotypic progenitor adhesion at 10 s contact time. Data is presented as a box-whisker plot. Median is black and mean is white. (**d**) Slope of contact region ('contact stiffness') extracted from the approach trace versus F_{max} recorded for each force-distance curve. Grey squares, no statistical correlation was seen ($r = 0.14$); five arbitrarily chosen curves for each progenitor types are highlighted as coloured circles. (**e**) F_{max} for homotypic adhesion at 10 s contact in control (Ca^{2+}), EGTA (5 mM)-treated or *E-cadherin*-morpholino oligonucleotide expressing (–cdh1; 8 ng per embryo) progenitors. (**f**) Sagittal section of the dorsal germ-ring margin of a shield stage wild-type embryo (6 hpf; schematic drawing in upper left corner) fluorescently stained with an E-cadherin antibody. Picture was taken by confocal microscopy. (**f′**) Western blot analysis and quantification (bar chart) of the amount of biotinylated, membrane-bound classical cadherins (pan-Cadherin antibody) in dissociated progenitors normalized to total tubulin ($n = 4$; median ± MAD). Scale bar in (**f**), 50 μm. Numbers above or below square brackets indicate *P* values for the corresponding combinations.

Dictyostelium discoideum, fibroblasts and white blood cells have shown that actomyosin contraction and cell-cortex tension are directly related to each other[12–14]. We therefore determined cell-cortex tension of different germ-layer progenitors as a read-out of their specific actomyosin activity. To measure cell-cortex tension, we deformed the surface of single progenitors with a colloidal force probe and recorded the resulting force-indentation curves with an AFM (Fig. 2a). Cell-cortex tension was extracted from force-indentation curves using the cortical shell-liquid core or liquid droplet model[13] (for details see Methods). We found that ectoderm progenitors had the highest cell-cortex tension, followed by mesoderm and then endoderm progenitors (Fig. 2b–d). To determine whether these differences in cell-cortex tensions were due to differential actomyosin activity, we measured cell-cortex tension of germ-layer progenitors in the presence of blebbistatin (see Methods for details), a specific inhibitor of myosin II activity. Exposure to blebbistatin reduced cell-cortex tension to the same level in all progenitor types (Fig. 2d). Together, these findings demonstrate that progenitors show differential actomyosin-dependent cell-cortex tension.

The factors regulating cell-cortex tension of germ-layer progenitors are poorly understood. Nodal/TGFβ signalling is known to be required and sufficient to induce mesoderm and endoderm cell fates and morphogenesis[15]. Thus, to test whether Nodal/TGFβ signalling can modulate cell-cortex tension of progenitors, we measured cortex tension of ectoderm progenitors exposed to recombinant activin, a Nodal-related TGFβ signal previously shown to function as a mesendoderm inducer and dorsalizer[16]. In ectoderm progenitors cultured for 120 min in the presence of activin (100 ng ml^{-1}), cell-cortex tension was significantly lower than in untreated cells (untreated = 54.5 ± 8.6 μN m^{-1}, $n = 32$; treated = 21.7 ± 8.6 μN m^{-1}, $n = 32$; median ± MAD; $P = 2.2\times10^{-16}$). This suggests that actomyosin-dependent cell-cortex tension of germ-layer progenitors can be modulated by Nodal/TGFβ-related signalling.

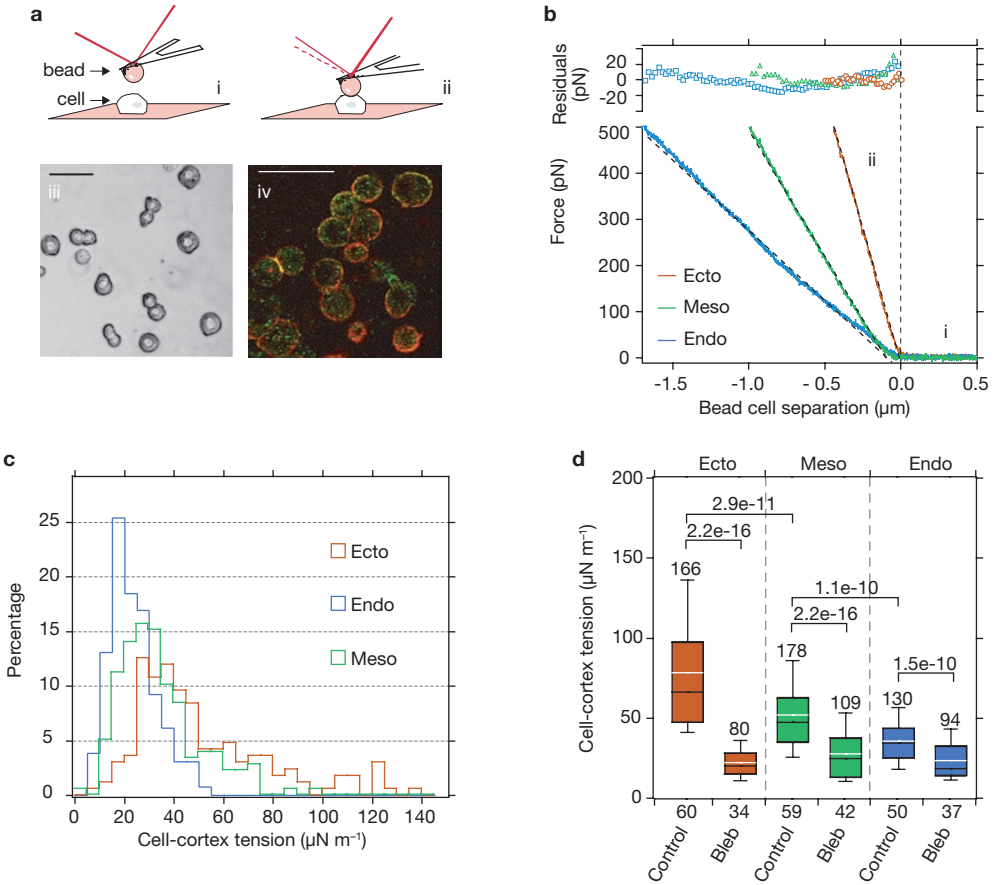

Figure 2 Cell-cortex tension of germ-layer progenitors measured by SCFS. (**a**) Principle of the indentation experiment. A passivated colloidal force probe (bead; diameter = 5 μm) is moved towards a given progenitor cell (cell) at 1 μm s^{-1} (i) and the cell surface is deformed by the bead (ii). (iii) Phase-contrast micrograph of typical progenitors used for measurements. (iv) Phalloidin (actin; red) and anti-phospho-myosin antibody (green) staining of fixed mesoderm progenitors after 3 h in culture. Scale bars in iii and iv, 50 μm. (**b**) Representative force curves for progenitor cells are shown and fitted to a linear model to extract the cell-cortex tension. The upper panel shows the residuals of the fit. (**c**) Distribution of cell-cortex tension for ectoderm, endoderm and mesoderm progenitors. (**d**) Box-whisker plot of cell-cortex tension for different progenitor cell types in the presence or absence of blebbistatin (bleb, 50 μM). Median is black and mean is white. Sample size is indicated over each box and number of tested cells below the *x* axis. Numbers above brackets indicate *P* values for the corresponding combinations.

To correlate our measurements of adhesion and cell-cortex tension with the actual sorting behaviour of germ-layer progenitors, we performed a series of *in vitro* cell sorting experiments (Fig. 3a). We have shown previously that ectoderm and mesendoderm cells sort efficiently when mixed in primary culture, resulting in an ectoderm cluster surrounded by mesendoderm cells[17]. Applying the same methodology to all three germ-layer progenitor types, we found that when ectoderm cells were mixed with either mesoderm or endoderm cells, ectoderm cell clusters became surrounded by mesoderm ($n = 56$ aggregates) or endoderm cells ($n = 45$) after 17 h in culture (Fig. 3b–f). Cell sorting also occurred in mixed mesoderm and endoderm cell populations after 17 h in culture with mesoderm clusters completely ($n = 27$) or partially ($n = 29$) enveloped by endoderm cells (Fig. 3g). Importantly, germ-layer progenitor aggregation began immediately after seeding and cell sorting was already evident minutes after mixing (Fig. 3h). This suggests that the cell–cell contact times used in our adhesion assay (Fig. 1b) are relevant for the actual sorting behaviour of progenitors. A sorting order of germ-layer progenitors thus exists *in vitro*; ectoderm cells are surrounded by mesoderm or endoderm cells and mesoderm cells are surrounded by endoderm cells. Analogous configurations and sorting orders have been reported for dissociated germ-layer progenitors of *Rana pipiens* embryos[18].

That higher actomyosin-dependent cell-cortex tension (Fig. 2b–d), but not cohesion (Fig. 1c), correlates with ectoderm progenitor sorting to the inside of a heterotypic aggregate (Fig. 3e, f), suggests that cell-cortex tension, rather than cohesion, promotes progenitor sorting to the inside. To test whether actomyosin-dependent cell-cortex tension is required for progenitor sorting, we exposed mixed ectoderm and mesoderm (or endoderm) progenitors to drugs that perturb actomyosin activity. We found that mixed ectoderm and mesoderm (as well as endoderm) progenitors failed to sort efficiently when exposed to cytochalasin D (an actin depolymerizer) or (–)-blebbistatin (an inhibitor of myosin II activity; Fig. 3i, j, l, m; Supplementary Information, Fig. S3c), but not to (+)-blebbistatin (an inactive enantiomer, Supplementary Information, Fig. S3a). Similarly, no sorting occurred in the presence of BDM, a myosin inhibitor (Supplementary Information, Fig. S3b). Importantly, relative differences in homotypic cell–cell adhesion between the different progenitor types remained unchanged in the

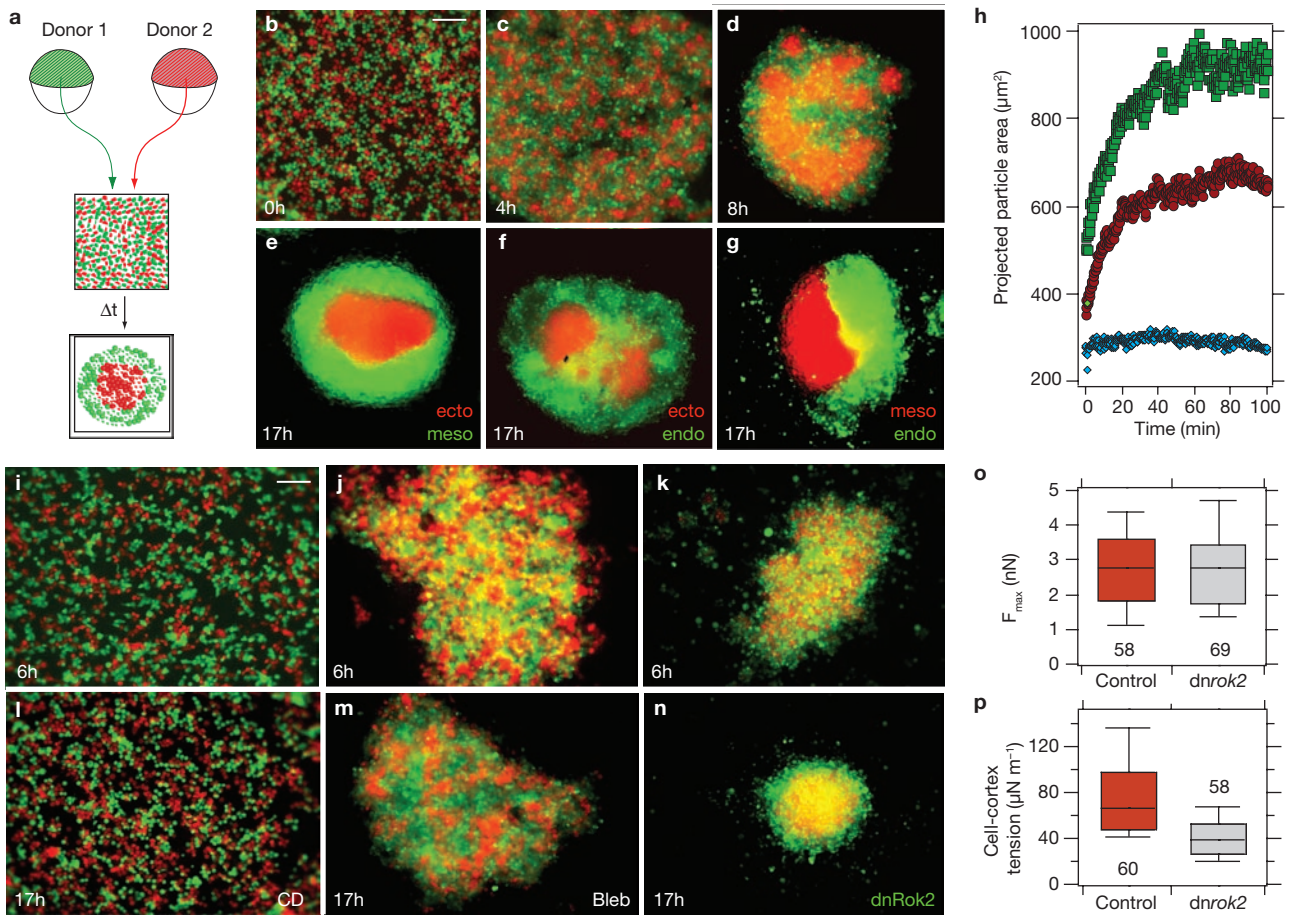

Figure 3 Sorting of germ-layer progenitors *in vitro* (**a**) Schematic drawing of an *in vitro* progenitor cell sorting assay. Two different embryos were dissociated and progenitors were mixed in a hanging drop. Cell sorting was observed after 17 h in culture. (**b**–**e**) Sorting of mesoderm and ectoderm co-culture at different time-points. (**f**, **g**) Sorting of ectoderm-endoderm (**f**) and mesoderm-endoderm (**g**) co-cultures after 17 h in culture. (**h**) Time-course of cell sorting in an ectoderm-mesoderm co-culture. The cluster size (projected particle area) increased immediately after seeding without any detectable lag-phase (ectoderm, red circles; mesoderm, green squares), whereas no increase in cluster size was observed in the presence of EDTA (blue diamonds). Generally, progenitor cell aggregates after 17 h in culture did not show obvious signs of cell differentiation (as judged by marker gene expression; data not shown; ref. 17), indicating that they retain their progenitor cell identities. (**i**, **j**, **l**, **m**) Hanging drop co-cultures of ectoderm (red) and mesoderm (green) progenitor cells in the presence of cytochalasin D (10 mM, **i**, **l**) or (–)-blebbistatin (50 μM, **j**, **m**) after 6 h (**i**, **j**) and 17 h (**l**, **m**) in culture. (**k**, **n**) Hanging drop co-culture of untreated ectoderm cells and ectoderm cells obtained from embryos injected with 350 pg/embryo of dn*rok2* mRNA to reduce cortex tension after 6 h (**k**) and 17 h (**n**) in culture. (**o**) SCFS measurements of ectoderm cell cohesion (10 s contact time; $P = 0.923$). (**p**) Cell-cortex tension in control and dn*rok2* mRNA expressing cells (350 pg/embryo; $P = 2.2 \times 10^{-16}$). Number of tested cells are given below or above the boxes. Scale bars in (**b**, **i**), 300 μm. Epifluorescence microscopy images were constructed in ImageJ.

presence of (–)-blebbistatin (Supplementary Information, Fig. S2f), indicating that blebbistatin functions in cell sorting by perturbing cell-cortex tension (Fig. 2d) rather than adhesion. Together, these findings show that differential actomyosin-dependent cell-cortex tension is required for efficient progenitor cell sorting.

To determine whether differential actomyosin-dependent cell-cortex tension is also sufficient to drive germ-layer progenitor cell sorting, we interfered selectively with actomyosin activation in ectoderm progenitors and then analysed their sorting behaviour when mixed with untreated ectoderm, mesoderm or endoderm cells. To cell-autonomously interfere with actomyosin activation, a dominant-negative version of Rho kinase 2 (dnRok2), an upstream regulator of actomyosin activity[19], was expressed. DnRok2-expressing ectoderm progenitors showed reduced cell-cortex tension, whereas cohesion remained unchanged (Fig. 3o, p) and, when mixed with untreated ectoderm, mesoderm or endoderm cells, sorted to the outside of heterotypic aggregates (Fig. 3k, n; Supplementary Information, Fig. S3d, f). Similar results were obtained by expressing a dominant-negative version of myosin regulatory light chain 2a (dnMRLC2a), a downstream target of Rok2, to reduce cortex tension (Supplementary Information, Fig. S3e). This suggests that differential actomyosin- dependent cell-cortex tension is sufficient to direct progenitor cell sorting.

To explain the sorting behaviour of germ-layer progenitors in the context of our adhesion and tension measurements, we simulated progenitor cell sorting using the Cellular Potts Model[20,21]. In this model, cell behaviour is driven by energy minimization whereby the total energy of an aggregate depends on the interfacial tension between cell-to-cell and cell-to-medium interfaces[3,22]. The interfacial tension between two cells is determined by the adhesion (J_{ij}) between the cell types *i* and *j*, and by the cortex elasticity and cortex tension (T_i and T_j) of the two cells[3,23].

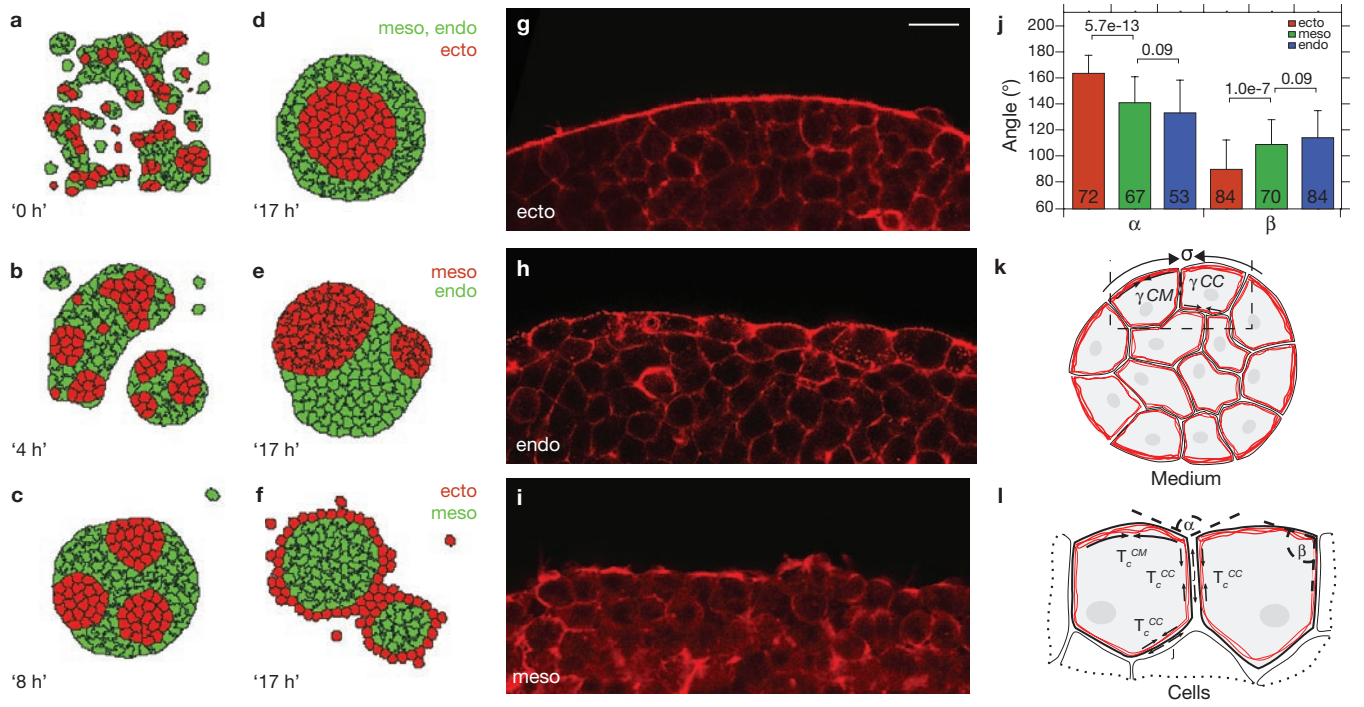

Figure 4 Simulations of germ-layer progenitor cell sorting using the Cellular-Potts-Model and germ-layer explant surface analysis. (**a**–**d**) Progenitor cell sorting in an aggregate consisting of ectoderm (red) and mesoderm (or endoderm) cells (green) at consecutive stages of sorting. (**e**) Stable configuration of mesoderm (red)-endoderm (green) aggregates. (**f**) Stable configuration of ectoderm (red)-mesoderm (green) aggregates with reduced cell-cortex tension in ectoderm cells. (**g**–**k**) Germ-layer explant surface analysis. (**g**–**i**) Actin (phalloidin)-staining of ectoderm (**g**), endoderm (**h**) and mesoderm (**i**) explants. Similar results for actin localization were observed using FITC-labelled actin monomers (data not shown). (**j**) Summary of the two angles α and β between two cells at the surface of a homotypic aggregate (for angle representation see **l**). Data are mean ± s. d. Validity of the angle measurement was confirmed with 0.5α + β = 180 ± s. d.; actual *P* values are given above the brackets; number of observations are within the bars. (**k**) Aggregate surface tension (results from the difference between the interfacial tension at the cell-to-cell (γ^{CC}) and cell-to-medium (γ^{CM}) interface. (**l**) The cellular origin of interfacial tension. At the cell-to-cell interface, the tension γ^{CC} is increased by the cortical tension T_c^{cc} of both cells, and decreased by the adhesion energy *J*. At the cell-to-medium interface there is no adhesion, thus the interfacial tension γ^{CM} is equal to the cortical tension T_c^{cm}. The surface tension σ is therefore increased by cell-cortex tension at the cell-to-medium interface and the adhesion between the cells within the aggregate. Scale bar in **g**, 20 μm.

Relative values for adhesion were similar to those measured in Fig. 1c with homotypic adhesion ($J_{endo} > J_{meso} > J_{ecto}$) and heterotypic adhesion ($J_{ecto,meso} = J_{ecto,endo} = J_{meso,endo}$ = homotypic adhesion J_{ecto}). Adhesion of cells to the medium was set to zero.

We simulated progenitor cell sorting using two different conditions: in the first case, cell-cortex tension was assumed to be homogeneous for the whole cell, independent of interactions with other cells or the medium (interface-independent tension). Relative tension values were set according to the experimental data shown in Fig. 2d with $T_c^{ecto} > T_c^{meso} > T_c^{endo}$. In the second case, we regarded the tension measurements of Fig. 2d as representative of only the cell-to-medium interface, as proposed previously[11], with $T_c^{ecto/medium} > T_c^{meso/medium} > T_c^{endo/medium}$ (interface-specific tension). In contrast, cortex tension at cell-to-cell interfaces was equal for all progenitor types.

When we simulated tissue self-assembly under conditions of interface-independent tension, ectoderm cells enveloped both mesoderm and endoderm progenitors (data not shown), contrary to our experimental observations (Fig. 3b–e). In contrast, under conditions of interface-specific tension, progenitors sorted exactly as observed in the experiments, with mesoderm and endoderm progenitors surrounding ectoderm (Fig. 4a–d) and ectoderm progenitors with reduced cortex tension surrounding mesoderm progenitors (Fig. 4f). This suggests that interfacial energy resulting from adhesion and cell-cortex tension can trigger germ-layer progenitor sorting if differential cortex tension exists at the cell-to-medium interface.

To determine whether differences in actomyosin-dependent cell-cortex tension exist at the cell-to-medium interface, we stained ectoderm, mesoderm and endoderm tissue explants after 7 h in culture with the F-actin marker phalloidin. All explants showed uniform intensity of cortical actin staining at cell-to-cell interfaces, whereas elevated actin staining was seen at the cell-to-medium interface (the surface of the explants; Fig. 4g–i). In addition, the surface of ectoderm explants was straighter (Fig. 4j) and displayed higher cortical actin levels than mesoderm and endoderm explants (Fig. 4g–i), suggesting higher tension at the cell-to-medium interface of ectoderm explants. Together, these findings support the prediction from our simulations that cortex tension at the cell-to-medium interface is different between ectoderm and mesoderm cells. The findings are also consistent with our previous observations that tissue surface tension is higher in ectoderm versus mesendoderm explants[17].

Questions remain as to the relevance of progenitor sorting *in vitro* for their actual morphogenetic behaviour *in vivo*. To compare progenitor sorting *in vitro* and *in vivo*, we therefore established an *in vivo* cell sorting assay system. We transplanted ectoderm, mesoderm or endoderm progenitors into the blastoderm margin of maternal-zygotic *one-eyed-pinhead* (*MZ-oep*) mutant embryos, which consist predominantly of ectoderm progenitors[16], and then monitored the sorting behaviour

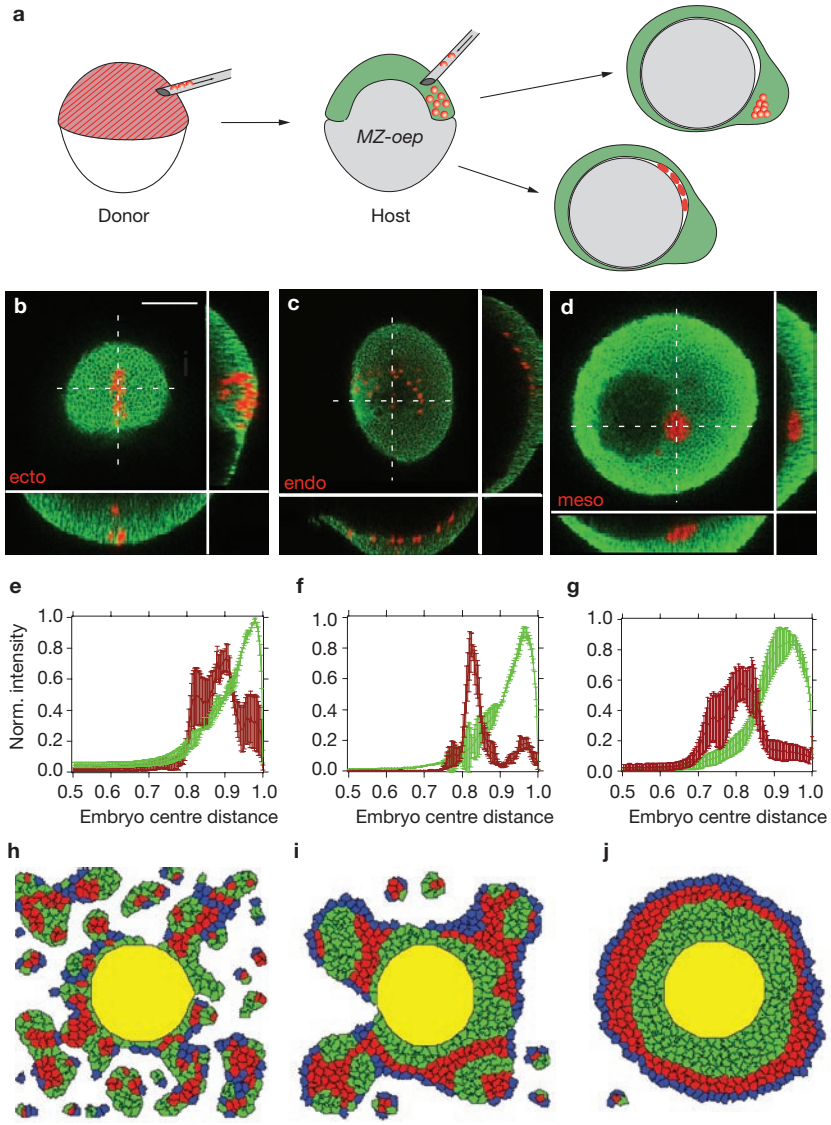

Figure 5 Sorting of germ-layer progenitor cells *in vivo* (**a**) Schematic drawing of an *in vivo* progenitor cell sorting assay. Progenitor cells from different embryos (donor, red) were transplanted into an *MZ-oep* mutant embryo (host, green) at shield stage (6 hpf) and sorting of donor and host cells was observed at bud stage (10 hpf). Two different possible outcomes are represented schematically: spreading of donor cells between epiblast and yolk or integration of donor cells into the epiblast of the host embryo. (**b**–**d**) Localization of donor ectoderm ($n = 9$ embryos; **b**), endoderm ($n = 7$; **c**) and mesoderm ($n = 7$; **d**) progenitor cells in *MZ-oep* mutant embryos at bud stage. Dorsal views. Images were constructed in Leica SP5 LAS software. (**e**–**g**) Analysis of the spatial configuration of transplanted donor (red) and host (green) cells depicted as normalized (norm.) intensity as a function of the distance from the centre of the embryo. Ectoderm cells overlapped more strongly with host tissues compared with mesoderm and endoderm cells. (**h**–**j**) Simulation of consecutive steps of progenitor cell sorting in the presence of extra-embryonic EVL and yolk cell. Adhesion and tension values for mesoderm and ectoderm progenitors were set as in Fig. 4. We further assumed that EVL cells adhere preferentially to ectoderm progenitors ($J_{evl,ecto} > J_{evl,meso}$), that yolk and EVL cells have uniform contraction (not interface-specific) and that the adhesion between yolk and the germ-layer progenitors is equal to the homotypic adhesion of germ-layer progenitors ($J_{yolk,meso} = J_{meso,meso}$, $J_{yolk,ecto} = J_{ecto,ecto}$). This results in mesoderm progenitors adhering more strongly to the yolk than do ectoderm progenitors. Progenitor cell sorting was simulated with one big yolk cell (yellow) mixed with 10% EVL cells (blue), 45% ectoderm (red) and 45% mesoderm (green) progenitors. Similarly to the *in vivo* situation, EVL cells were found at the outside, yolk at the centre and ectoderm cells surrounding mesoderm. Scale bar in **b**, 150 μm.

between the transplanted donor cells and the host cells of the recipient embryo (Fig. 5a). When ectoderm progenitors were transplanted into *MZ-oep* embryos at shield stage (6 hpf), they remained as a loosely coherent cluster of donor cells embedded in the epiblast of the host embryo at bud stage (10 hpf; Fig. 5b, e). In contrast, when mesoderm or endoderm progenitors were transplanted into the germ-ring of a shield stage *MZ-oep* host embryo, they segregated from the host cells and either arranged into a compact cell cluster (mesoderm; Fig. 5d, g) or dispersed as single cells (endoderm; Fig. 5c, f) between the yolk cell and the overlying epiblast at bud stage. These experiments suggest that *in vitro* and *in vivo* sorting of germ-layer progenitors retains common and divergent features. In both cases, ectoderm progenitors segregate from mesoderm and endoderm progenitors into distinct cell clusters that contact each other. However, the position of ectoderm relative to mesoderm and endoderm differs; ectoderm is on the inside of heterotypic aggregates *in vitro*, but more superficial to mesoderm and endoderm *in vivo*.

The apparent discrepancy in the final positioning of germ-layer progenitors is probably due to progenitor sorting *in vivo* being influenced by interactions with extra-embryonic tissues such as the enveloping cell layer (EVL) on the outside of the embryo and the yolk cell on the inside (initial source of Nodal signals), which are not present in our *in vitro* preparations. To test this hypothesis, we simulated progenitor cell sorting in the presence of the yolk cell and EVL cells. Assuming both strong adhesion of ectoderm progenitors to the EVL[24] and mesoderm cells to the yolk syncytial layer (YSL)[5], progenitor sorting was similar to that *in vivo* (Fig. 5h–j; Supplementary Information, Fig. S4), suggesting that our progenitor adhesion and tension measurements can predict the *in vivo* sorting order when additional parameters, such as EVL or yolk-cell adhesion are included. This view is also supported by experiments showing that when the blastoderm margin is removed from the embryo and placed in culture, endogenous mesendoderm and ectoderm, in the absence of EVL and yolk, self-assemble into an inside-out configuration, similarly to the *in vitro* sorting experiments[17].

The Differential Adhesion Hypothesis[26], one of the most prevalent hypotheses in the field, proposes that cell sorting and tissue organization result from disparate adhesiveness of the participating cells. Here we show that differential intercellular adhesion of germ-layer progenitors alone is not sufficient to explain their sorting behaviour and that differences in actomyosin-dependent cell-cortex tensions are critical. How can differences in cortex tension between progenitor types influence their sorting behaviour? Cells sort according to their aggregate surface tension: the aggregate with the lower surface tension surrounds the one with the higher surface tension. Aggregate surface tension (σ) characterizes the tendency of the global aggregate surface area to decrease. It is therefore increased by the tension at the interface between cells and the medium (γ^{CM}, the tendency of each cell to decrease its cell-to-medium contact area) and decreased by the tension at the interface between cells (γ^{CC}, the tendency of each cell to decrease its cell-to-cell contact area; Fig. 4k; ref. 22). Thus high tension at the cell-to-medium interface in combination with low tension at the cell-to-cell interface causes high aggregate surface tension. Tension at the cell-to-cell interface (γ^{CC}), in turn, is the result of cortical tension minus adhesion at this interface, whereas tension at the cell-to-medium interface (γ^{CM}) is determined by cortical tension only (Fig. 4l; refs 23, 27). For cell-cortex tension to increase aggregate surface tension and to influence sorting behaviour, it must increase the difference between γ^{CC} and γ^{CM}: it must be higher at the cell-to-medium interface than the cell-to-cell interface. Similarly, cell-cell adhesion increases aggregate surface tension by diminishing cell-to-cell tension. It is thus important that both interface-specific cortex tension and differential adhesion should be taken into account to explain progenitor sorting[27].

Whether differential adhesion and tension are the only factors determining progenitor sorting *in vivo*, or whether other factors such as directed cell migration, epithelialization and extracellular matrix deposition, are also involved, remains to be determined. Notably, none of the forming germ layers in zebrafish show obvious epithelial characteristics or clearly localized extracellular matrix depositions[9], leaving directed cell migration as the most likely process to function together with adhesion and tension in germ-layer organization. Future experiments analysing the specific migratory behaviour of germ-layer progenitors will be required to reveal the relative contribution of cell migration to germ-layer formation during zebrafish gastrulation. □

METHODS

Injections of mRNA and morpholino oligonuclotides. To generate endoderm or mesoderm progenitors, one-cell-stage wild-type *tub longfin* embryos were injected with *casanova* (*cas*) mRNA (50 pg) or *cyclops* (*cyc*) mRNA (100 pg) and *cas* morpholino oligonucleotides (2 ng; GeneTools), respectively[28,29]. For ectoderm progenitors, *MZ-oep* were used[16]. The specific identity of germ-layer progenitors was determined by *in situ* staining of the injected embryos (Supplementary Information, Fig. S1a–p). Embryos injected with *cas* mRNA ubiquitously expressed the endoderm marker *Sox17* (ref. 28), suggesting that cells were fated to become endoderm. We confirmed that the results obtained with *cas*-expressing cells were due to their endoderm character rather than being a specific effect of *cas* overexpression by showing similar adhesive and tensile properties in progenitors from embryos ubiquitously expressing dominant active da*TARAM-A* (50 pg), previously shown to induce endoderm cell fate upstream of *cas*[28] (Supplementary Information, Fig. S1q, r). Embryos injected with *cyc* mRNA and *cas* morpholino oligonucleotides ubiquitously expressed *goosecoid*, a marker of anterior axial mesoderm, suggesting that they were fated to become anterior axial mesoderm. In general, these injections allowed efficient induction of different progenitor types with many[28,29], but not necessarily all features of their endogenous counterparts.

Adhesion measurements. Plasma-activated cantilevers (Veeco MLCT, nominal spring constant $k = 30$ mN m^{-1}) were incubated with concanavalin A (ConA, 2.5 mg ml^{-1}, Sigma) overnight at 4°C and carefully rinsed in PBS before use. Plasma-activated microscope slides (GoldSeal) were prepared using a two-well coating mask (nAmbition) to obtain an adhesive and non-adhesive substrate. One well was filled with 50 µl heat-inactivated fetal calf serum (Invitrogen), ensuring passivation of the surface (non-adhesive substrate), whereas the other was filled with 50 µl ConA (2.5 mg ml^{-1}; adhesive substrate). Before the experiment, substrates were gently rinsed with the cell culture medium used to perform the adhesion tests (CO_2-independent DMEM/F-12 1:1 buffered in 15 mM Hepes and supplemented with penicillin (100 U ml^{-1}) and streptomycin (0.1 mg ml^{-1})). Diluted cell suspensions were then seeded onto the substrate. All experiments were carried out at 25°C. For homotypic adhesion experiments, cells were selected using phase-contrast microscopy. For heterotypic adhesion experiments, one-cell-stage embryos were injected with both mRNA (see above) and either FITC- or TRITC-coupled dextran (Molecular Probes). Cells were identified using fluorescence microscopy. A given 'probe'-cell (Fig. 1a) was selected from the non-adhesive side of the substrate with a ConA-coated cantilever by gently pressing on it with a controlled force of 1 nN for typically 1 s. The cell was raised from the surface for 2–10 min to firmly attach to the cantilever. The probe-cell was then moved above a 'target'-cell that was firmly attached to the adhesive ConA-coated part of the substrate. Adhesion experiments ('force-distance cycles', see Fig. 1a) were performed using a 1 nN contact force, 10 µm s^{-1} approach and retract velocities, and contact times ranging from 1–60 s. Contact time was varied randomly for a given couple to prevent any systematic bias or history effect. Each condition (that is, same probe-target couple at same contact time) was repeated up to three times, with a resting time of 30 s between successive contacts. Each probe-cell was used to test several target-cells. No more than 40 curves were taken with any given probe-cell. Cells were observed continuously during and between the force-distance cycles to judge whether they were intact and stably associated with the cantilever/substrate. Only cells that showed characteristic 'ruffling' behaviour and pseudopod formation were used. Target-cell pictures were taken to measure diameter and observe morphology. Force-distance curves were analysed using IgorPro custom-made routines to extract maximum adhesion force (Fig. 1b) and cell deformation (Fig. 1d) during the contact. Data were then pooled and statistically processed as described in Supplementary Information. Cadherin-dependence of cell adhesion was tested after depleting calcium by adding EGTA (5 mM, Sigma) to the medium, or injecting embryos with *E-cadherin* morpholino oligonucleotides (8 ng; Fig. 1e). To reduce actomyosin function, cells were pre-incubated in (–)-blebbistatin (50 µM, Sigma). Experiments were carried out in 5 µM (–)-blebbistatin with no more than 15–20 repeated measures taken with a single probe-cell because of mechanical fragility of the treated cells. Preparation of E-cadherin-coated substrates was carried out as described previously[8]. Approach and retract velocities were set to 4 µm s^{-1}.

Cell-cortex tension measurements and liquid droplet model assumptions. Colloidal force probes were prepared by attaching a glass bead (5 µm diameter, Kisker Biotech) to a cantilever (Veeco MLCT) using a two-component Araldit epoxy glue. Such beads were used as an indenter to create a large and smooth contact geometry

with the cell, hence reducing the strain induced by the pressure during contact[30]. To prevent non-specific adhesion to the cells, the modified cantilevers were either incubated with heat inactivated fetal calf serum (Invitrogen) or silanized (1% methyltriethoxysilane (Sigma) in hexane (Fluka) for 1 h) and then passivated with 1% pluronic F127 (Sigma) in ultrapure water. The cells were seeded on a glass substrate. Force-distance curves were acquired using 500 pN contact force and 1 μm s^{-1} approach/retract velocity and indentation; δ, was calculated from tip displacement (Fig. 2b). Up to three curves, with at least 15 s waiting time between successive curves, were taken per cell to prevent any history effect[30]. To describe the mechanics of the different cell types by AFM indentation, the approach of Rosenbluth *et al.*[31] was chosen. The liquid droplet model[13] was applied to extract the cell-cortex tension, as previously proposed for different cell lines using the micropipette technique[13,14,32]. Cell-cortex tension is influenced directly by the state of the contractile apparatus of the cell[12,14]. The liquid droplet model describes the cell as a viscous cytosol surrounded by an elastic (actin-based) cortex. This is based on the following assumptions: 1) an actin cortex exists in close proximity to the cell membrane, and the nucleus occupies only a small volume of the cell; 2) cells are not adherent and spherical; 3) force versus indentation curves are linear (see equation below); 4) indentation depth is small, compared with the size of the cell; 5) cell-cortex tension is independent of the cantilever speed; 6) cells have a large plasma-membrane reservoir., Cell-cortex tension T_c can then be calculated using the following equation[32]:

$$F = \left[2T_c\left(\frac{1}{R_c}+\frac{1}{R_b}\right)\times 2\pi R_b\right]\times\delta$$

(F = force, δ = indentation, R_c = cell radius and R_b = bead radius). Phalloidin staining of our progenitors showed an actin-based cortex both in dissociated cells and in embryos (Fig. 2a). The ratio of cell- to nucleus- volume estimated from phase-contrast images was high (21 ± 12, mean ± s. d.). Dissociated cells were roughly spherical (Figs. 2a; Supplementary Information, Fig. S2c) and weakly adherent to the substrate. Force versus indentation curves were linear (70% of all curves) for a large range of indentation values (Fig. 2b), with the deformation (max ~ 1 μm) being at least one order of magnitude smaller than the cell diameter (approximately 18–20 μm). Furthermore, we did not find a strong influence of the cantilever speed on cell-cortex tension (data not shown). Finally, our adhesion measurements suggest that the cells possess a large membrane reservoir as indicated by long lipid tubes extracted during the separation process using SCFS (tethers, Fig. 1a). Together, this provides experimental support for using the liquid drop model to analyse our indentation experiments and gain information about the cortex tension of the progenitor types. To determine cell-cortex tension using the equation above, we used a force versus indentation line-fit between 125 pN and 250 pN to exclude errors that could be introduced while determining the bead-to-cell contact point[33]. Bead and cell radii were determined by phase-contrast microscopy. To alter cortex tension, cells were pre-incubated in (–)-blebbistatin (50 μM) or recombinant activin (100 ng ml^{-}1, Sigma) for 2 h. For blebbistatin, cells were measured in the presence of 5 μM (–)-blebbistatin. All experiments were performed at 25°C.

Note: Supplementary Information is available on the Nature Cell Biology website.

ACKNOWLEDGEMENTS

We thank Pierre Bongrand, Wayne Brodland, Jonne Helenius, Mathias Köppen, Andy Oates, Ewa Paluch, Laurel Rohde, Erik Schäffer, Clemens Franz, Sylvia Schneider, Petra Stockinger, Anna Taubenberger, Florian Ulrich and Simon Wilkins for fruitful discussions; Stan Marée for sharing the simulation code for the Cellular-Potts-Model; Lara Carvalho for sharing unpublished results; JPK Instruments for technical support; Jonne Helenius for supporting data analysis procedures and the fifth floor seminar club for vibrant discussions. This work was supported by grants from the Boehringer Ingelheim Fonds to M. K., Deutsch-Französische Hochschule to M. K. and P. H. P. and the Deutsche Forschungsgemeinschaft to C. P. H.

AUTHOR CONTRIBUTIONS

M. K. performed and analysed the AFM and biochemical experiments and the hanging drop cell aggregation/sorting experiments; Y. A. performed the molecular biology experiments, embryo injections, cell culture work (sorting and explant analysis), cell transplantations and *in situ* hybridizations; J. K. performed the simulation experiments and contributed to image analysis; C. P. H., D. M., F. G. and P. H. P. conceived and designed the experiments; M. K., C. P. H., D. M. and P. H. P. prepared the manuscript.

Published online at http://www.nature.com/naturecellbiology/
Reprints and permissions information is available online at http://npg.nature.com/reprintsandpermissions/

1. Tepass, U., Godt, D. & Winklbauer, R. Cell sorting in animal development: Signalling and adhesive mechanisms in the formation of tissue boundaries. *Curr. Opin. Genet. Dev.* **12,** 572–582 (2002).
2. Montero, J. A. & Heisenberg, C. P. Gastrulation dynamics: Cells move into focus. *Trends Cell Biol.* **14,** 620–627 (2004).
3. Brodland, G. W. The differential interfacial tension hypothesis (dith): a comprehensive theory for the self-rearrangement of embryonic cells and tissues. *J. Biomech. Eng.* **124,** 188–197 (2002).
4. Benoit, M., Gabriel, D., Gerisch, G. & Gaub, H. E. Discrete interactions in cell adhesion measured by single-molecule force spectroscopy. *Nature Cell Biol.* **2,** 313–317 (2000).
5. Puech, P. H., Poole, K., Knebel, D. & Muller, D. J. A new technical approach to quantify cell-cell adhesion forces by afm. *Ultramicroscopy* **106,** 637–644 (2006).
6. Zhang, X. *et al.* Atomic force microscopy measurement of leukocyte-endothelial interaction. *Am. J. Physiol. Heart Circ. Physiol.* **286,** H359–367 (2004).
7. Gumbiner, B. M. Regulation of cadherin-mediated adhesion in morphogenesis. *Nature Rev. Mol. Cell Biol.* **6,** 622–634 (2005).
8. Ulrich, F. *et al.* Wnt11 functions in gastrulation by controlling cell cohesion through Rab5c and E-cadherin. *Dev. Cell* **9,** 555–564 (2005).
9. Montero, J. A. *et al.* Shield formation at the onset of zebrafish gastrulation. *Development* **132,** 1187–1198 (2005).
10. Geiger, B. *et al.* Broad spectrum pan-cadherin antibodies, reactive with the C-terminal 24 amino acid residues of N-cadherin. *J. Cell Sci.* **97,** 607–614. (1990).
11. Harris, A. K. Is cell sorting caused by differences in the work of intercellular adhesion? A critique of the steinberg hypothesis. *J. Theor. Biol.* **61,** 267–285 (1976).
12. Dai, J., Ting-Beall, H. P., Hochmuth, R. M., Sheetz, M. P. & Titus, M. A. Myosin I contributes to the generation of resting cortical tension. *Biophys. J.* **77,** 1168–1176 (1999).
13. Evans, E. & Yeung, A. Apparent viscosity and cortical tension of blood granulocytes determined by micropipet aspiration. *Biophys. J.* **56,** 151–160 (1989).
14. Thoumine, O., Cardoso, O. & Meister, J. J. Changes in the mechanical properties of fibroblasts during spreading: A micromanipulation study. *Eur. Biophys. J.* **28,** 222–234 (1999).
15. Schier, A. F. Nodal signaling in vertebrate development. *Annu. Rev. Cell Dev. Biol.* **19,** 589–621. (2003).
16. Gritsman, K. *et al.* The EGF–CFC protein one-eyed pinhead is essential for nodal signaling. Cell **97,** 121–132 (1999).
17. Schötz, E.-M. *et al.* Quantitative differences in tissue surface tension influence zebrafish germ layer positioning *HFSP J.* **2,** 42–56 (2008).
18. Davis, G. S., Phillips, H. M. & Steinberg, M. S. Germ-layer surface tensions and "tissue affinities" in *Rana pipiens* gastrulae: quantitative measurements. *Dev. Biol.* **192,** 630–644 (1997).
19. Marlow, F., Topczewski, J., Sepich, D. & Solnica-Krezel, L. Zebrafish Rho kinase 2 acts downstream of Wnt11 to mediate cell polarity and effective convergence and extension movements. *Curr. Biol.* **12,** 876–884 (2002).
20. Maree, A. F. M., Grieneisen, V. A. & Hogeweg, P. The Cellular Potts Model and biophysical properties of cells, tissues and morphogenesis. in *Single Cell-Based Models in Biology and Medicine* (eds Anderson, A. R. A., Chaplain, M. & Rejniak, K. A.) 107–136 (Birkhäuser Verlag, Basel; 2007).
21. Ouchi, N. B., Glazier, J. A., Rieu, J.-P., Upadhyaya, A. & Sawada, Y. Improving the realism of the cellular potts model in simulations of biological cells. *Physica A: Stat. Mech. Applic.* **329,** 451–458 (2003).
22. Graner, F. Can surface adhesion drive cell-rearrangement? Part I: Biological cell-sorting. *J. Theoret. Biol.* **164,** 455–476 (1993).
23. Kafer, J., Hayashi, T., Maree, A. F. M., Carthew, R. W. & Graner, F. Cell adhesion and cortex contractility determine cell patterning in the *Drosophila* retina. *Proc. Natl Acad. Sci. USA* **104,** 18549–18554 (2007).
24. Shimizu, T. *et al.* E-cadherin is required for gastrulation cell movements in zebrafish. *Mech. Dev.* **122,** 747–763 (2005).
25. Warga, R. M. & Kane, D. A. A role for N-cadherin in mesodermal morphogenesis during gastrulation. *Dev. Biol.* **310,** 211–225 (2007).
26. Steinberg, M. S. Differential adhesion in morphogenesis: A modern view. *Curr. Opin. Genet. Dev.* **17,** 281–286 (2007).
27. Lecuit, T. & Lenne, P. F. Cell surface mechanics and the control of cell shape, tissue patterns and morphogenesis. *Nature Rev. Mol. Cell Biol.* **8,** 633–644 (2007).
28. Aoki, T. O. *et al.* Molecular integration of casanova in the nodal signalling pathway controlling endoderm formation. *Development* **129,** 275–286 (2002).
29. Carmany-Rampey, A. & Schier, A. F. Single-cell internalization during zebrafish gastrulation. *Curr. Biol.* **11,** 1261–1265 (2001).
30. Dimitriadis, E. K., Horkay, F., Maresca, J., Kachar, B. & Chadwick, R. S. Determination of elastic moduli of thin layers of soft material using the atomic force microscope. *Biophys. J.* **82,** 2798–2810 (2002).
31. Rosenbluth, M. J., Lam, W. A. & Fletcher, D. A. Force microscopy of nonadherent cells: A comparison of leukemia cell deformability. *Biophys. J.* **90,** 2994–3003 (2006).
32. Lomakina, E. B., Spillmann, C. M., King, M. R. & Waugh, R. E. Rheological analysis and measurement of neutrophil indentation. *Biophys. J.* **87,** 4246–4258 (2004).
33. Crick, S. L. & Yin, F. C. Assessing micromechanical properties of cells with atomic force microscopy: Importance of the contact point. *Biomech. Model. Mechanobiol.* **6,** 199–210 (2007).

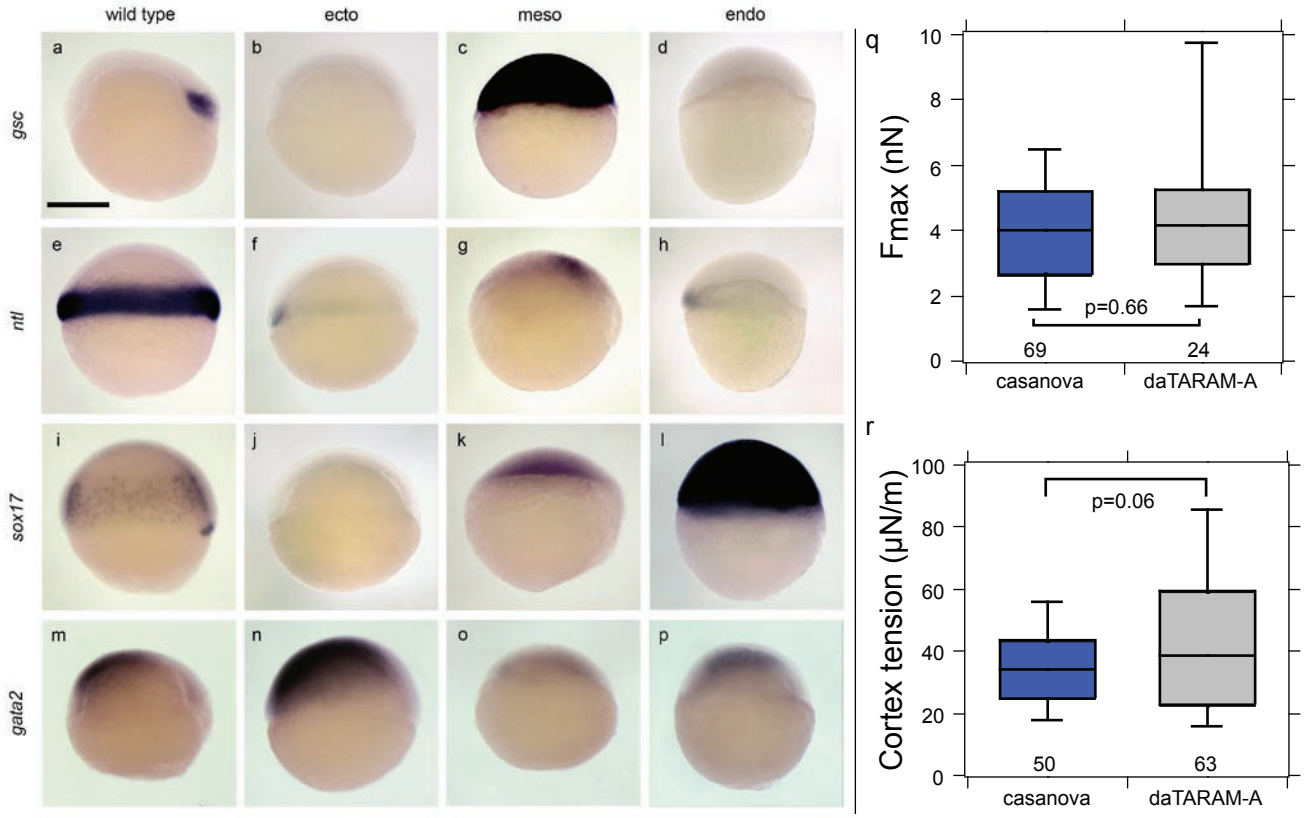

Figure S1 Germ layer progenitor cell identities. Whole mount *in situ* hybridization for *gsc* (anterior axial mesoderm-prechordal plate; **a-d**), *ntl* (mesoderm; **e-h**), *sox17* (endoderm; **i-l**) and *gata2* (ventral ectoderm; **m-p**) expression in wild type (**a,e,i,m**), *MZ-oep* (ecto; **b,f,j,n**), *cyc m*RNA+*cas MO* (meso; **c,g,k,o**), and *cas m*RNA (endo; **d,h,l,p**) injected embryos. Scale bar in (**a**)=250 µm. (**q,r**) Endoderm progenitor cell adhesion and tension induced by dominant active *TARAM-A*. F_{max} for homotypic adhesion (q) and cortex tension (r) of endoderm cells obtained by expressing either *cas m*RNA (50 pg/embryo) or dominant active *TARAM-A m*RNA (da*TARAM-A*; 50 pg/embryo). Actual *p*-values are given above/below the brackets, number of observations below the whiskers.

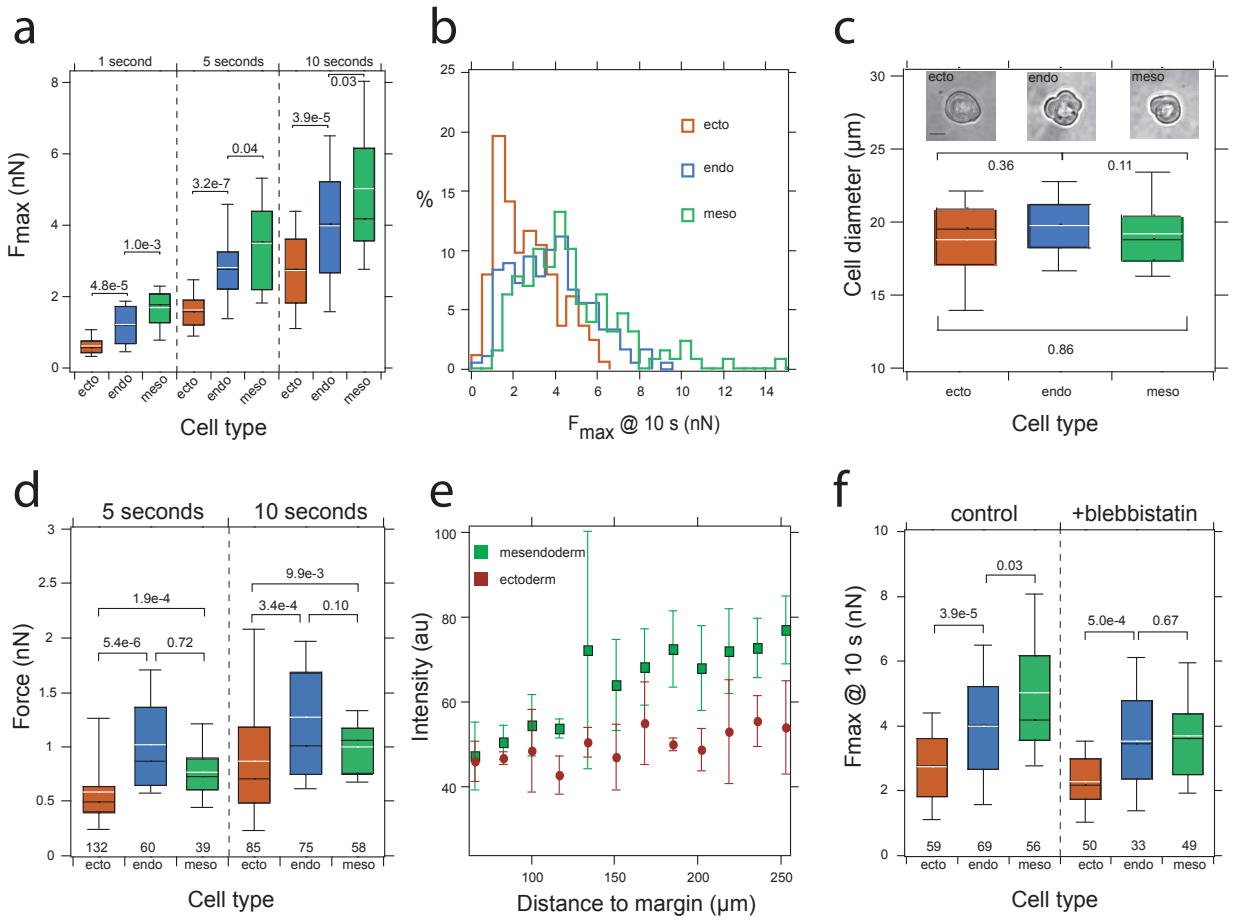

Figure S2 Germ layer progenitor cell adhesion and cell size (**a**) F_{max} of homotypic progenitor cell adhesion as a function of contact time displayed as box-whisker plots. Median in black and mean in white. Numbers above/below brackets indicate *p* values for the corresponding combinations. (**b**) Distribution of F_{max} for the three progenitor cell types at 10 s contact time. Unprocessed raw data; binning set to 500 pN. (**c**) Box-whisker plot of the cell diameter for different progenitor cell types. Numbers above/below brackets indicate *p* values for the corresponding combinations. Phase contrast micrographs of typical progenitor cell morphology used in the SCFC experiments are shown above the box-whisker plots. Scale bar: 10 µm. (**d-f**) Involvement of Cadherin and Myosin in progenitor cell adhesion. (**d**) F_{max} as a function of contact time for progenitor cell adhesion to an E-cadherin-coated surface. (**e**) Intensity profile of E-cadherin staining in the hypoblast (mesoderm and endoderm progenitors) and epiblast (ectoderm progenitors) determined from Fig.1f. E-cadherin plasma membrane intensities are higher in cells of the anterior axial hypoblast compared to adjacent epiblast cells. (**f**) Quantification of F_{max} for homotypic adhesion as a function of germ layer progenitor cell type in the presence or absence of Blebbistatin at 10 s contact time. Actual *p*-values are given above the brackets, number of observations below the whiskers.

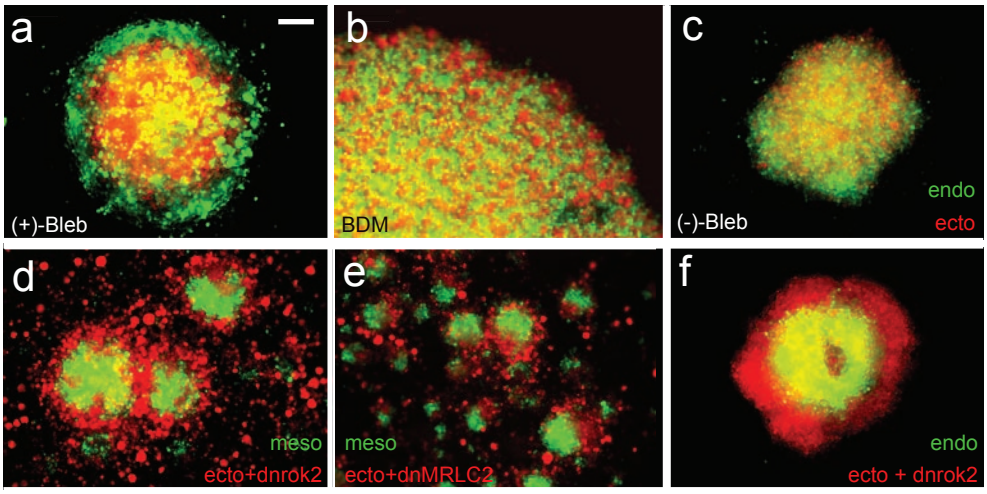

Figure S3 Germ layer progenitor cell sorting and cortex tension. (**a,b**) Sorting in mesoderm (green) and ectoderm (red) hanging drop co-cultures in the presence of 50 μM (+)-Blebbistatin (**a**) and 20mM BDM (**b**) after 17 h in culture. (**c**) Sorting of ectoderm (red) and endoderm (green) in hanging drop co-cultures in the presence of (-)-Blebbistatin after 17 h in culture. (**d-f**) Sorting in mesoderm-ectoderm (**d,e**) and endoderm-ectoderm (**f**) hanging drop co-cultures with ectoderm cells (red) expressing either dn*rok2 m*RNA (**d,f**; 350 pg/embryo) or dn*mrlc2a m*RNA (**e**; 250 pg/embryo) to reduce cortex tension after 17 h in culture. Scale bar in (**a**)=150 μm. Images were constructed in ImageJ.

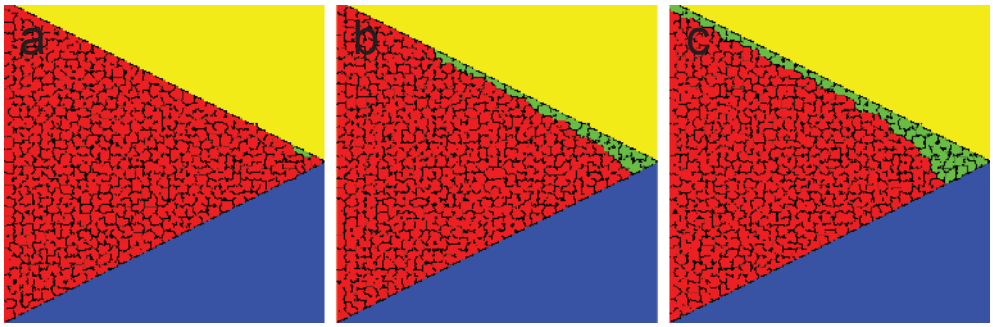

Figure S4 Simulation of germ layer progenitor cell sorting in the presence of extra-embryonic EVL and yolk cell. Adhesion and tension values for mesoderm and ectoderm progenitors were set as in Fig.4. We further assumed that EVL cells adhere preferentially to ectoderm progenitors ($J_{evl,ecto}>J_{evl,meso}$), that yolk and EVL cells do have uniform contraction (not interface-specific) and that the adhesion between yolk and the germ layer progenitors is equal to the homotypic adhesion of germ layer progenitors ($J_{yolk,meso}=J_{meso,meso}$, $J_{yolk,ecto}=J_{ecto,ecto}$). (**a-c**) Simulation of consecutive steps of progenitor cell sorting at the germ ring margin with the yolk (yellow) and EVL (blue) positions fixed, the space between yolk and EVL filled with ectoderm cells (red), and the rightmost ectoderm cell differentiating into a mesoderm cell (green) at regular intervals. Similar to the situation at the germ ring margin, mesoderm progenitors disperse between the ectoderm and yolk.

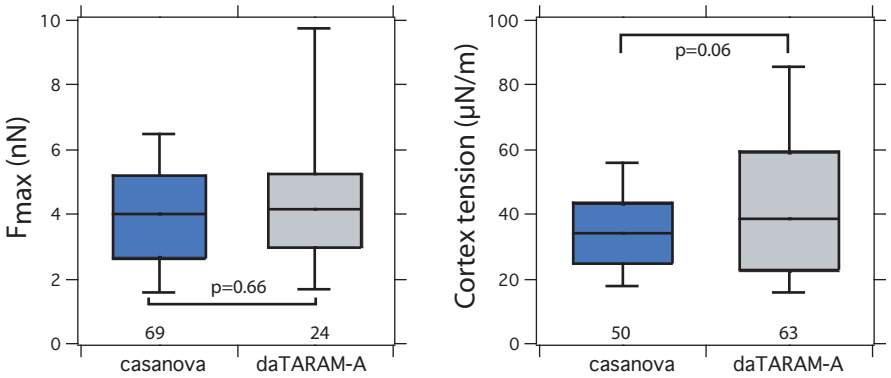

Figure S5 Endoderm progenitor cell adhesion and tension. F_{max} for homotypic adhesion (a) and cortex tension (b) of endoderm cells obtained by expressing either *cas* *m*RNA (50 pg/embryo) or dominant active *TARAM-A* *m*RNA (da*TARAM-A*; 50 pg/embryo). Actual *p*-values are given above/below the brackets, number of observations below the whiskers.

Table S1 Summary of SCFS data for homotypic and heterotypic germ layer progenitor cell adhesion. Separation forces (F_{max}; presented as median±MAD in pN) and the number of force curves/cells are given as a function of contact times and progenitor cell types.

		1sec		5sec	
condition	**cell type**	**median±mad**	**# of curves(cells)**	**median±mad**	**# of curves(cells)**
homo	**ecto**	575±165	137(35)	1580±323	119(39)
	endo	1203±527	86(23)	2772±531	89(32)
	meso	1778±368	91(32)	3531±1148	110(42)
hetero	**ecto vs meso**	969±268	60(22)	2316±702	64(22)
	ecto vs endo	729±258	68(23)	1901±561	89(29)
	endo vs meso	866±251	58(20)	2436±683	53(21)
egta	**ecto**	143±40	38(10)	212±35	34(10)
	endo	196±31	22(7)	254±50	35(9)
	meso	175±60	43(14)	281±57	45(13)
cdh1	**ecto**	254±37	37(11)	328±83	65(18)
	endo	422±118	75(22)	592±156	86(25)
	meso	378±100	67(20)	746±307	61(18)

		10sec		20sec	
condition	**cell type**	**median±mad**	**# of curves(cells)**	**median±mad**	**# of curves(cells)**
homo	**ecto**	2767±925	162(59)	3458±918	85(32)
	endo	4028±1310	168(69)	5748±2205	79(44)
	meso	4178±1199	127(56)	5979±1926	44(29)
hetero	**ecto vs meso**	2963±643	89(33)	3575±1354	49±(18)
	ecto vs endo	2743±934	101(32)	2631±893	43(14)
	endo vs meso	2630±731	70(28)	2706±715	37(16)
egta	**ecto**	284±32	50(15)	240±51	21(8)
	endo	286±92	39(12)	279±65	29(8)
	meso	252±93	46(14)	342±106	41(14)
cdh1	**ecto**	441±126	52(16)	445±175	59(17)
	endo	698±219	100(30)	625±292	89(28)
	meso	892±338	75(23)	1389±515	63(19)